Letter

Thermal decoupling of deuterium and tritium during the inertial confinement fusion shock-convergence phase

N. V. Kabadi,* R. Simpson, P. J. Adrian, A. Bose, J. A. Frenje, M. Gatu Johnson, B. Lahmann, C. K. Li, C. E. Parker, F. H. Séguin, G. D. Sutcliffe, and R. D. Petrasso
Massachusetts Institute of Technology Plasma Science and Fusion Center, Cambridge, Massachusetts 02139, USA

S. Atzeni
Dipartimento SBAI, Universit'a degli Studi di Roma "La Sapienza," Via Antonio Scarpa 14, 00161, Roma, Italy

J. Eriksson
Department of Physics and Astronomy, Uppsala University, SE-752 37 Uppsala, Sweden

C. Forrest, S. Fess, V. Yu Glebov, R. Janezic, O. M. Mannion, H. G. Rinderknecht, M. J. Rosenberg, and C. Stoeckl
University of Rochester Laboratory for Laser Energetics, Rochester, New York 14623, USA

G. Kagan
Centre for Inertial Fusion Studies, The Blackett Laboratory, Imperial College, London SW7 2AZ, United Kingdom

M. Hoppe, R. Luo, M. Schoff, and C. Shuldberg
General Atomics, San Diego, California 92121, USA

H. W. Sio, J. Sanchez, L. Berzak Hopkins, D. Schlossberg, K. Hahn, and C. Yeamans
Lawrence Livermore National Laboratory, Livermore, California 94550, USA

(Received 19 January 2021; accepted 23 June 2021; published 15 July 2021)

A series of thin glass-shell shock-driven DT gas-filled capsule implosions was conducted at the OMEGA laser facility. These experiments generate conditions relevant to the central plasma during the shock-convergence phase of ablatively driven inertial confinement fusion (ICF) implosions. The spectral temperatures inferred from the DTn and DDn spectra are most consistent with a two-ion-temperature plasma, where the initial apparent temperature ratio, $\frac{T_T}{T_D}$, is 1.5. This is an experimental confirmation of the long-standing conjecture that plasma shocks couple energy directly proportional to the species mass in multi-ion plasmas. The apparent temperature ratio trend with equilibration time matches expected thermal equilibration described by hydrodynamic theory. This indicates that deuterium and tritium ions have different energy distributions for the time period surrounding shock convergence in ignition-relevant ICF implosions.

DOI: 10.1103/PhysRevE.104.L013201

In inertial confinement fusion (ICF) implosions, the goal is to implode a spherical capsule to reach high densities and temperatures necessary to achieve a burning plasma state. In both direct and indirect-drive ICF, the compression is initiated by a series of shocks traversing the dense cryogenic fuel layer. These shocks coalesce near the shell-gas interface and propagate through the lower density ($\sim$0.3 mg/cm^3) central gas as a single strong shock ($M \sim 10$). The shock strengthens as it converges. Near shock convergence and rebound, there is a period in which the central plasma is in a low-density high-temperature state and the hydrodynamic assumption of high collisionality breaks down. Subsequently the dense outer shell continues to converge, increasing the central density and initiating the primary nuclear burn [1].

Strong spherical shocks are prevalent not only in ICF plasmas, but also in astrophysical plasmas. In these systems, the postshocked material has equilibration timescales and mean free paths that are comparable to or larger than the system scale [2–4]. This indicates a potentially collisionless regime where different ion species could have independent dynamics based on their individual species properties: charge and mass. Previous experiments that used shock-driven D^{3}He gas-filled implosions to study the shock-convergence phase indicated the presence of spatial disequilibrium (species separation), thermal disequilibrium (thermal decoupling) of the ion species, and absolute yield degradation [2,5–8]. Other experiments have implicated species separation and multi-ion physics as the cause of anomalous fusion yields in compressive implosions, and these phenomena may originate from the preceding shock phase [9–13]. These results indicate that an understanding of all phases of an ICF implosion,

*kabadi@mit.edu

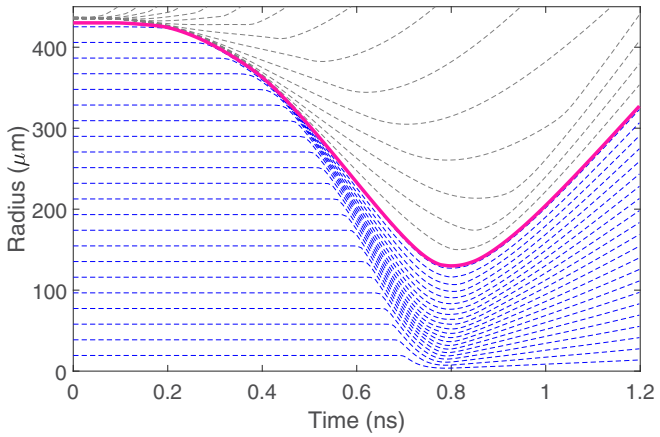

FIG. 1. DUED simulated *r-t* plot for the 4 mg/cm^3, 50:50 D:T, Omega shot 89931. The thick solid magenta curve is the shell-hotspot interface. Below this the blue dashed curves indicate the 50:50 DT central plasma control mass trajectories, and the above dashed gray curves represent the SiO_2 shell.

including the shock-convergence phase, is necessary to reach ignition [14].

Present modeling and experiments rely heavily on average-ion hydrodynamic simulations, which cannot capture multi-ion dynamics. Simulations that solve the Fokker-Planck equation to capture multi-ion and kinetic dynamics exist [15,16] and have advanced the field in recent years, but they are still computationally expensive. Other multi-ion hydrodynamic simulations are becoming available, but are not the standard for ICF computations. A basic understanding of the important multi-ion physics could allow better implosion modeling without dramatically increasing the computational overhead. In this Letter, experimental results from DT gas-filled shock-driven implosions are used to develop a physical model for thermal decoupling and ion-ion equilibration during the ICF shock-convergence phase.

A series of experiments using DT gas-filled shock-driven implosions was carried out at the Omega Laser facility [17]. The capsules were nominally 2.3-μm thick glass shells with an 860-μm outer diameter that were driven by a 0.6-ns square laser pulse delivering 15 kJ. These experiments generated conditions relevant to the shock-convergence phase of hotspot ignition experiments such as those conducted at the National Ignition Facility (NIF), without being complicated by a subsequent compression phase. This is shown in the radius vs time plot in Fig. 1, where lines show the trajectories of control mass elements within the simulation. After shock rebound($\sim$0.75 ns) the system quickly begins to disassemble with very little shell-driven compression. The plotted trajectories are from a DUED [18] simulation of OMEGA shot 89931 which was a 4 mg/cm^3 50:50 D:T gas-filled implosion. This simulation includes real ion viscosity and overpredicted the measured DTn yield by only $\sim$10%, indicating that it properly captures the fuel dynamics. For lower density implosions DUED does progressively worse at predicting the nuclear yields indicating that kinetic and multi-ion effect are becoming increasingly important at lower density [2]. A summary table showing this trend is included in the Supplemental Material [19]. With a high ablation rate and minimal residual shell mass, implosions of this type are insensitive to hydrodynamic instabilities [20]. The experimental platform is very similar to previous D^{3}He gas-filled shock-driven implosions [2,5,7].

By conducting experiments with DT fuel, results are immediately comparable to the shock-convergence phase of ignition-relevant implosions, which all use a DT gas fill. Another key advantage of DT as compared to D^{3}He is the relative impact of emission weighting. In DT-filled implosions the primary nuclear products are the fusion deuterium-deuterium and deuterium-tritium neutrons (DD-n and DT-n) from which the apparent temperatures of the D and T ions are inferred. At high temperatures (>10 keV) the reactivity for DT and DD fusion are similar functions of temperature; therefore the DD-n and DT-n are emitted from similar volumes in space and time [21]. This is not the case for deuterium-helium-3 protons (D^{3}He-p) and DD-n, or DT-n and DD-n at lower temperatures, which can be emitted from substantially different volumes due to the large difference in their temperature dependencies. For the lower temperature more hydrolike DT implosions included in this study, a higher order analytical model accounting for this emission weighting is used.

DT-gas-filled implosions with a range of initial fill densities (0.2–4 mg/cm^3) and fill ratios (40%–97% D) were conducted on OMEGA. In addition, data from shock-driven indirect-drive exploding pushers (IDEPs) conducted at the NIF are used [22]. In these experiments, the spectral DTn and DDn ion temperatures (T_{sDTn} and T_{sDDn}) are inferred from the width of the produced neutron spectra as measured by neutron time-of-light (NTOF) diagnostics [23,24]. NTOFs and nuclear activation detectors were used to determine the neutron yields [23]. These measured quantities are included in the Supplemental Material [19]. As previously discussed, to infer the level of thermal decoupling at high ion temperature the apparent species temperatures (T_T and T_D) can be inferred directly from the measured spectral temperatures based on the species masses (m_D and m_T) [25], without accounting for emission weighting due to temperature profiles.

$$T_D = T_{\mathrm{sDDn}}, \tag{1}$$

$$T_T = T_{\mathrm{sDTn}} + \frac{m_D}{m_T}(T_{\mathrm{sDTn}} - T_{\mathrm{sDDn}}). \tag{2}$$

These relations are purely a kinematic correction and do not account for variations in the reactivity. They are valid so long as the ratio of the two temperatures is between 0.5 and 2 as demonstrated with Monte Carlo calculations in the Supplemental Material [19]. For moderate temperature implosions the method demonstrated in [26] is used to directly infer the apparent temperature ratio necessary to match T_{sDTn} and T_{sDDn} as well as the measured yield ratio, while accounting for spatial and temporal temperature variation to second order. For the IDEPs, the uncertainty in the inferred apparent temperature ratio is dominated by the model and estimated based on the inferred temperature variation [26].

The differential equation governing the change in temperature of an ion species within a two-species plasma due to ion-ion equilibration is given by [27]

$$\frac{dT_2}{dt} = \frac{1}{\tau_{21}}(T_1 - T_2), \tag{3}$$

where τ_{21} is the characteristic time at which species 2 equilibrates with species 1, which can be calculated as

$$\tau_{21} = 5.6 \times 10^{18} \frac{(m_1 T_2 + m_2 T_1)^{3/2}}{Z_1^2 Z_2^2 (m_1 m_2)^{1/2} n_1 \lambda_{12}} \text{sec}. \quad (4)$$

Here, Z_j is the charge of ion species j in units of the proton charge, n_j the ion number densities, T_j the ion temperatures in eV, and λ is the Coulomb logarithm. All unspecified units are cgs. Then the differential equation describing the evolution of the temperature ratio can be written as

$$\frac{d}{dt}\frac{T_2}{T_1} = -\frac{1}{\tau_{12}}\left(\frac{T_2}{T_1}\right)^2 + \left(\frac{1}{\tau_{12}} - \frac{1}{\tau_{21}}\right)\frac{T_2}{T_1} + \frac{1}{\tau_{21}}. \quad (5)$$

The solution to this equation, when ignoring the weak dependence on species fraction, can be written as

$$\frac{T_2}{T_1} = \tanh\left(\frac{t}{\tau_{ii}} + \text{atanh}(R_0)\right), \quad (6)$$

where the integration constant, R_0, is the temperature ratio as t goes to 0 and the total equilibration time is given by the harmonic mean of the τ_{12} and τ_{21}:

$$\tau_{ii} = 2\left[\frac{1}{\tau_{12}} + \frac{1}{\tau_{21}}\right]^{-1}. \quad (7)$$

This dynamic model can be applied to the average observables from an implosion under certain assumptions: the heating mechanism happens at a discrete point in time; an average timescale can be used to capture the time between nuclear emission and heating; and heat loss mechanisms do not substantially affect the apparent temperature ratio. In these shock-driven implosions, the ions are predominantly heated by the shock near convergence and rebound. Nuclear emission onset occurs near shock rebound making the width of the emission history a good average timescale to capture the time between shock coupling and measurement of the nuclear observables. In these implosions, the FWHM of the DTn emission history (τ_{DTn}) was measured using the neutron temporal diagnostic [28]. To estimate τ_{ii}, the density is inferred from the minimum shell radius as measured by time-resolved x-ray framing cameras [29]. The ratio of τ_{ii} to τ_{DTn} should dictate the level of thermal disequilibrium. The ratio of the measured τ_{DTn} to τ_{ii} for different initial fill densities and ratios of DT-filled implosions are shown in the Supplemental Material [19].

$$\tau_N = \frac{\tau_{\text{DTn}}}{\tau_{ii}}. \quad (8)$$

Figure 2 shows the apparent ratio of T_T to T_D plotted versus τ_N for three different D:T fill ratios. The observed trend is consistent for all fill fractions and well described by the equation

$$\frac{T_T}{T_D} = \tanh\left[\tau_N + \text{atanh}(1.52_{\pm 0.04})\right], \quad (9)$$

which indicates a trend that begins from a value of ≈ 1.5 and decays to 1 (or thermal equilibrium) at a rate dictated by τ_N. Since the initial temperature ratio will be dominated by shock coupling based on ion-species properties, we can conclude that the shock coupling scales linearly with mass (D and T have identical charge).

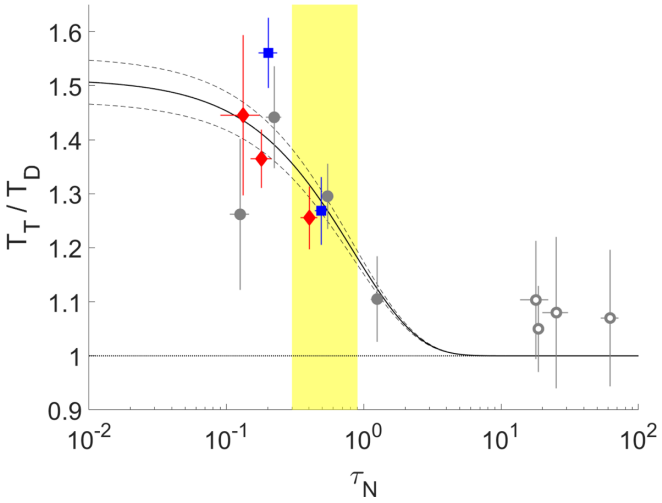

FIG. 2. Apparent temperature ratio versus the normalized equilibration timescale for DT gas-filled implosions. Red diamonds are 97:3, gray circles 50:50, and blue squares 40:60 D:T atomic fill ratio. The unfilled gray circles are from NIF IDEPs. All points are consistent with the equation $\frac{T_T}{T_D} = \tanh[\tau_N + \text{atanh}(1.52_{\pm 0.04})]$ shown by the solid black curve with dashed 95% confidence interval. The reduced chi-square statistic for this fit is 0.96. The yellow-shaded region represents the conditions most relevant to the shock-convergence phase in NIF ICF implosions.

$$T_i \propto m_i. \quad (10)$$

Coupling directly proportional to mass is consistent with the rebounding shock stagnating the incoming flow and converting the flow energy of a species into thermal energy. It is also consistent with predictions for the mass dependence of shock coupling [30,31] and recent astrophysical observations of collisionless shock heating [4].

The measured apparent temperature-ratio trend could potentially be explained by large flows, either random or radial, but this explanation can be ruled out as subsequently discussed. It has been shown that plasma flows with large variance along a line of sight can significantly broaden the measured fusion product spectra resulting in an increased apparent ion temperature [32]. The level of broadening is directly proportional to the total mass of the fusion products. In combination with the relations in Eqs. (1) and (2), this gives a maximal apparent temperature ratio of $\frac{T_T}{T_D} = 1.42$. In order to reach the observed value, all of the measured spectral broadening must come from bulk flow, requiring near zero thermal temperature. This is not plausible given the observed nuclear yields and velocity of the required flow to reach an apparent temperature ~20 keV. For the lowest density 50:50 DT implosions the DT yield was 5×10^{11}, the final number density was 6.9×10^{21} cm^{-3}, the minimum radius was 90 μm, and the emission history was 120 ps wide. This gives a rough estimate for the DT reactivity of 1.2×10^{16} cm^3/s, which would correspond to a 10 keV Maxwellian for a hydrodynamic system. The maximum simulated fluid velocity of any single cell is ~1000 km/s, which corresponds to an increase in apparent temperature of only ~6 keV. So at least

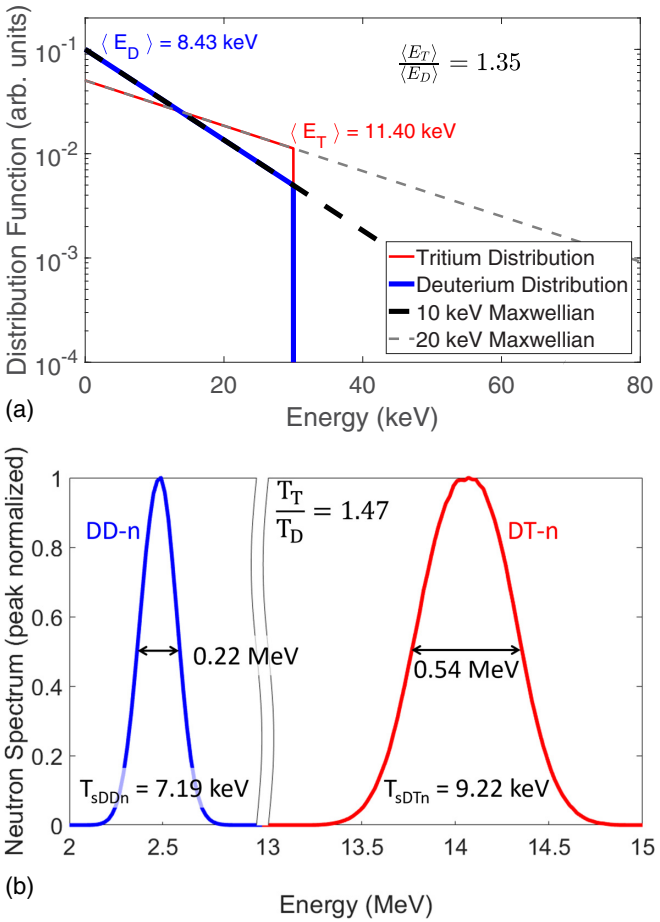

FIG. 3. (a) Truncated Maxwellian distribution functions used for the deuterium and tritium ions when calculating the fusion neutron spectra. The ratio of the tritium to deuterium mean energy is 1.35. (b) Monte Carlo simulated DD-n and DT-n spectra using the distribution functions in (a). The spectral ion temperatures inferred from the width of the neutron spectra are labeled next to each spectrum. The apparent tritium to deuterium temperature ratio is 1.47 for a 9% error compared to the input 1.35.

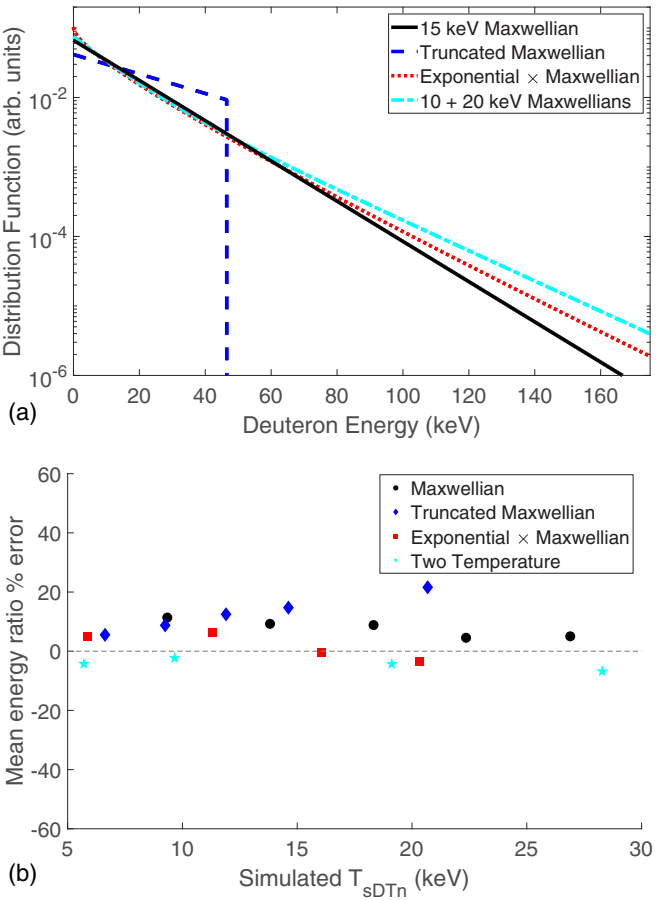

FIG. 4. (a) Various distribution functions used to compute resulting error in the inferred mean-energy ratio. Functions shown produce DD neutron spectra with widths that are similar to the 15 keV Maxwellian. (b) The error incurred when assuming the species mean-energy ratio is the apparent temperature ratio of T and D ions inferred from the DTn and DDn spectra produced by various distribution functions like the ones shown in (a).

10 keV of broadening comes from a thermal component and at most 6 keV from radial flow. Flows could certainly contribute to the apparent temperatures, but cannot explain the measured ratio at low density. For the lower-temperature high-density implosions, especially the NIF IDEPs, flows could potentially contribute to the apparent temperature ratio.

It should also be pointed out that it is possible the species do not have Maxwellian distribution functions as they are still equilibrating. It has been shown that ion tail depletion due to low ion-ion collisionality can significantly impact the spectral ion temperatures inferred from the width of fusion product spectra [33]. Such effects are difficult to quantify directly from the observables. For a Maxwellian distribution function, the apparent ion temperature fully characterizes an ion species' mean energy, and therefore a temperature ratio captures the mean energy ratio between two species. For non-Maxwellian distributions, the apparent temperature does not necessarily characterize a species mean energy, but an apparent temperature ratio still captures information about the ratio of the two species mean energies. To quantify the impact of various distribution functions on the apparent temperature ratio, the DT-n and DD-n energy spectra were computed using relativistic Monte Carlo calculations [34] while varying the shape of the distribution. In these calculations the distributions are isotropic. Distributions were varied such that an apparent temperature ratio ∼1.5 is inferred from the computed spectral temperatures at several mean energies. The standard deviations of the simulated neutron spectra were then used to infer spectral temperatures as though they were produced by Maxwellians. The spectral temperatures were analyzed in the same style as the data to infer an apparent temperature ratio. This ratio is compared to the known input mean-energy ratio for each calculation. An example of this process is shown in Fig. 3 for a truncated Maxwellian, meant to simulate the impact of complete loss of high-energy ions. In the shown example, the input mean energy ratio is 1.35 as shown in Fig. 3(a) while the apparent temperature ratio is 1.47 as shown in Fig. 3(b). In this example, the error incurred when assuming the apparent temperature ratio is the mean energy ratio is 9%. To mimic the potential effects of moderate loss of high-energy ions due to low collisionality, exponentially modified

Maxwellians were tested. Lastly, a two-temperature distribution was included. Examples of these distribution functions are shown in Fig. 4(a). Additional examples showing more details of these calculations are included in the Supplemental Material [19]. The resulting error in the apparent temperature ratio as compared to the mean energy ratio is plotted in Fig. 4(b). It is clear that even with significant changes to the high-energy ion population assuming the apparent temperature ratio is the species mean energy ratio results in at most 20% error. This indicates that the apparent temperature ratios plotted in Fig. 2 accurately quantify the mean energy ratio of the ion populations and the trend inferred from this plot is significant.

In summary, the apparent temperature trend and its explicit mass dependence is well represented by

$$\frac{T_2}{T_1} = \tanh\left[\tau_N + \operatorname{atanh}\left(\frac{m_2}{m_1}\right)\right], \tag{11}$$

$$\tau_N = \frac{\tau_{\mathrm{DTn}}}{\tau_{ii}} \propto \frac{(m_1 m_2)^{1/2}}{(m_1 T_2 + m_2 T_1)^{3/2}}. \tag{12}$$

This trend is valid for the measured DT and DD spectral temperatures across a variety of fill ratios and normalized equilibration timescales indicating that it properly captures the mass dependencies of the initial coupling and ion-ion thermal equilibration rate. The charge dependence of this coupling and equilibration cannot be investigated in these experiments as D and T have identical charge. The measurement of this mass dependence serves as the a laboratory-based experimental confirmation of long-standing predictions for shock heating in multi-ion plasmas [30,31] and agrees with recent astrophysical observations of collisionless shock heating [4]. Preferential heating of the higher mass species has been observed in simulations which include multiple ion species. In some cases it is seen that the thermal decoupling persists through nuclear emission [35]; in others they have equilibrated [36], consistent with the model of dynamic equilibration developed here. These results indicate that T and D ions spend substantial time out of thermal equilibrium between shock convergence and peak compression in ignition-relevant implosions at the NIF. While this thermal disequilibrium will not directly impact the hydrodynamic quantities of total pressure and density, higher order parameters can be strong functions of species temperature. One example is ion viscosity, which varies as $T_i^{5/2}$ [27]. In kinetic simulations, multi-ion effects including modifications to ion viscous heating have been observed to have significant impact on compression and fusion yields [16]. In average-ion hydrodynamic DUED simulations of 4 mg/cm^3 50:50 DT shock-driven implosions, removing real ion viscosity causes sharp temperature increases near shock convergence that increase the simulated yield by 50% and spectral ion temperature by 20% indicating that the absolute ion viscosity, and therefore species temperatures, are important for accurately simulating the conditions surrounding this phase. Hence the hotspot conditions, including thermal disequilibrium, at this time are critical as they set the initial conditions for the subsequent compression.

The data that support the findings of this study are available from the corresponding author upon reasonable request.

This material is based upon work supported by the Department of Energy, National Nuclear Security Administration under Awards No. DE-NA0003868 and No. DE-NA0003938. This report was prepared as an account of work sponsored by an agency of the United States Government. Neither the United States Government nor any agency thereof, nor any of their employees, makes any warranty, express or implied, or assumes any legal liability or responsibility for the accuracy, completeness, or usefulness of any information, apparatus, product, or process disclosed, or represents that its use would not infringe privately owned rights [37]. This work was performed under the auspices of the U.S. Department of Energy by Lawrence Livermore National Laboratory under Contract No. DE-AC52-07NA27344 and General Atomics under Contract No. DE-NA0001808.

[1] J. D. Lindl, P. Amendt, R. L. Berger, S. G. Glendinning, S. H. Glenzer, S. W. Haan, R. L. Kauffman, O. L. Landen, and L. J. Suter, Phys. Plasmas **11**, 339 (2004).

[2] M. J. Rosenberg, H. G. Rinderknecht, N. M. Hoffman, P. A. Amendt, S. Atzeni, A. B. Zylstra, C. K. Li, F. H. Séguin, H. Sio, M. G. Johnson *et al.*, Phys. Rev. Lett. **112**, 185001 (2014).

[3] S. Park, S. A. Zhekov, D. N. Burrows, G. P. Garmire, and R. McCray, Astrophys. J. **610**, 275 (2004).

[4] M. Miceli, S. Orlando, D. N. Burrows, K. A. Frank, C. Argiroffi, F. Reale, G. Peres, O. Petruk, and F. Bocchino, Nat. Astron. **3**, 236 (2019).

[5] H. G. Rinderknecht, M. J. Rosenberg, C. K. Li, N. M. Hoffman, G. Kagan, A. B. Zylstra, H. Sio, J. A. Frenje, M. Gatu Johnson, F. H. Séguin *et al.*, Phys. Rev. Lett. **114**, 025001 (2015).

[6] H. Sio, O. Larroche, S. Atzeni, N. V. Kabadi, J. A. Frenje, M. Gatu Johnson, C. Stoeckl, C. K. Li, C. J. Forrest, V. Glebov, P. J. Adrian, A. Bose, A. Birkel, S. P. Regan, F. H. Seguin, and R. D. Petrasso, Phys. Plasmas **26**, 072703 (2019).

[7] H. Sio, J. A. Frenje, A. Le, S. Atzeni, T. J. T. Kwan, M. Gatu Johnson, G. Kagan, C. Stoeckl, C. K. Li, C. E. Parker *et al.*, Phys. Rev. Lett. **122**, 035001 (2019).

[8] H. Rinderknecht, P. Amendt, M. Rosenberg, C. Li, J. Frenje, M. Gatu Johnson, H. Sio, F. Séguin, R. Petrasso, A. Zylstra *et al.*, Nucl. Fusion **57**, 066014 (2017).

[9] D. T. Casey, J. A. Frenje, M. Gatu Johnson, M. J.-E. Manuel, H. G. Rinderknecht, N. Sinenian, F. H. Séguin, C. K. Li, R. D. Petrasso, P. B. Radha *et al.*, Phys. Rev. Lett. **108**, 075002 (2012).

[10] J. R. Rygg, J. A. Frenje, C. K. Li, F. H. Séguin, R. D. Petrasso, J. A. Delettrez, V. Y. Glebov, V. N. Goncharov, D. D. Meyerhofer, S. P. Regan *et al.*, Phys. Plasmas **13**, 052702 (2006).

[11] H. W. Herrmann, J. R. Langenbrunner, J. M. Mack, J. H. Cooley, D. C. Wilson, S. C. Evans, T. J. Sedillo, G. A. Kyrala,

S. E. Caldwell, C. S. Young *et al.*, Phys. Plasmas **16**, 056312 (2009).
[12] S. C. Hsu, T. R. Joshi, P. Hakel, E. L. Vold, M. J. Schmitt, N. M. Hoffman, R. M. Rauenzahn, G. Kagan, X.-Z. Tang, R. C. Mancini *et al.*, Europhys. Lett. **115**, 65001 (2016).
[13] T. R. Joshi, S. C. Hsu, P. Hakel, N. M. Hoffman, H. Sio, and R. C. Mancini, Phys. Plasmas **26**, 062702 (2019).
[14] H. G. Rinderknecht, P. A. Amendt, S. C. Wilks, and G. Collins, Plasma Phys. Controlled Fusion **60**, 064001 (2018).
[15] O. Larroche, H. G. Rinderknecht, M. J. Rosenberg, N. M. Hoffman, S. Atzeni, R. D. Petrasso, P. A. Amendt, and F. H. Séguin, Phys. Plasmas **23**, 012701 (2016).
[16] W. T. Taitano, A. N. Simakov, L. Chacón, and B. Keenan, Phys. Plasmas **25**, 056310 (2018).
[17] T. R. Boehly, D. L. Brown, R. S. Craxton, R. L. Keck, J. P. Knauer, J. H. Kelly, T. J. Kessler, S. A. Kumpan, S. J. Loucks, S. A. Letzring *et al.*, Opt. Commun. **133**, 495 (1997).
[18] S. Atzeni, Comput. Phys. Commun. **43**, 107 (1986).
[19] See Supplemental Material at http://link.aps.org/supplemental/10.1103/PhysRevE.104.L013201 for additional experimental and simulated data.
[20] H. G. Rinderknecht, H. Sio, C. K. Li, A. B. Zylstra, M. J. Rosenberg, P. Amendt, J. Delettrez, C. Bellei, J. A. Frenje, M. Gatu Johnson *et al.*, Phys. Rev. Lett. **112**, 135001 (2014).
[21] H.-S. Bosch and G. M. Hale, Nucl. Fusion **32**, 611 (1992).
[22] S. Le Pape, L. Divol, L. Berzak Hopkins, A. Mackinnon, N. B. Meezan, D. Casey, J. Frenje, H. Herrmann, J. McNaney, T. Ma *et al.*, Phys. Rev. Lett. **112**, 225002 (2014).
[23] V. Y. Glebov, C. Stoeckl, T. C. Sangster, S. Roberts, G. J. Schmid, R. A. Lerche, and M. J. Moran, Rev. Sci. Instrum. **75**, 3559 (2004).
[24] D. H. Munro, J. E. Field, R. Hatarik, J. L. Peterson, E. P. Hartouni, B. K. Spears, and J. D. Kilkenny, Phys. Plasmas **24**, 056301 (2017).
[25] H. Brysk, Plasma Phys. **15**, 611 (1973).
[26] N. V. Kabadi, P. J. Adrian, A. Bose, D. T. Casey, J. A. Frenje, M. Gatu Johnson, B. Lahmann, O. M. Mannion, R. D. Petrasso, H. G. Rinderknecht, F. H. Séguin, H. W. Sio, G. D. Sutcliffe, and A. B. Zylstra, Phys. Plasmas **28**, 022701 (2021).
[27] S. I. Braginskii, Rev. Plasma Phys. **1**, 205 (1965).
[28] C. Stoeckl, R. Boni, F. Ehrne, C. J. Forrest, V. Y. Glebov, J. Katz, D. J. Lonobile, J. Magoon, S. P. Regan, M. J. Shoup *et al.*, Rev. Sci. Instrum. **87**, 053501 (2016).
[29] D. K. Bradley, P. M. Bell, J. D. Kilkenny, R. Hanks, O. Landen, P. A. Jaanimagi, P. W. McKenty, and C. P. Verdon, Rev. Sci. Instrum. **63**, 4813 (1992).
[30] Y. B. Zel'dovich and Y. P. Raizer, *Physics of Shock Waves and High-Temperature Hydrodynamic Phenomena* (Dover, New York, 2002), Vol. 2, pp. 515–520.
[31] B. D. Keenan, A. N. Simakov, W. T. Taitano, and L. Chacón, Phys. Plasmas **25**, 032103 (2018).
[32] T. J. Murphy, Phys. Plasmas **21**, 072701 (2014).
[33] G. Kagan, D. Svyatskiy, H. G. Rinderknecht, M. J. Rosenberg, A. B. Zylstra, C.-K. Huang, and C. J. McDevitt, Phys. Rev. Lett. **115**, 105002 (2015).
[34] J. Eriksson, S. Conroy, E. Andersson Sundén, and C. Hellesen, Comput. Phys. Commun. **199**, 40 (2016).
[35] C. Bellei, H. Rinderknecht, A. Zylstra, M. Rosenberg, H. Sio, C. K. Li, R. Petrasso, S. C. Wilks, and P. A. Amendt, Phys. Plasmas **21**, 056310 (2014).
[36] A. Le, T. J. T. Kwan, M. J. Schmitt, H. W. Herrmann, and S. H. Batha, Phys. Plasmas **23**, 102705 (2016).
[37] Reference herein to any specific commercial product, process, or service by trade name, trademark, manufacturer, or otherwise does not necessarily constitute or imply its endorsement, recommendation, or favoring by the United States Government or any agency thereof.